

# Analytic Approach for Controlling Quantum States in Complex Systems

Toshiya Takami

*Computing and Communications Center, Kyushu University, Fukuoka 812-8581, JAPAN*

Hiroshi Fujisaki

*Department of Chemistry, Boston University, 590 Commonwealth Ave., Boston, Massachusetts, 02215, USA\**

(Dated: July 15, 2018)

We examine random matrix systems driven by an external field in view of optimal control theory (OCT). By numerically solving OCT equations, we can show that there exists a smooth transition between two states called “moving bases” which are dynamically related to initial and final states. In our previous work [J. Phys. Soc. Jpn. **73** (2004) 3215-3216; Adv. Chem. Phys. **130A** (2005) 435-458], they were assumed to be orthogonal, but in this paper, we introduce orthogonal moving bases. We can construct a Rabi-oscillation like representation of a wavepacket using such moving bases, and derive an analytic optimal field as a solution of the OCT equations. We also numerically show that the newly obtained optimal field outperforms the previous one.

PACS numbers: 05.45.Mt, 02.30.Yy, 03.65.Sq

## I. INTRODUCTION

Controlling atomic and molecular processes by laser fields is one of current topics in physics and chemistry [1]. There are various control schemes applied to such processes:  $\pi$ -pulses [2], nonadiabatic transitions [3], adiabatic rapid passage [4], Stimulated Raman Adiabatic Passage (STIRAP) [5, 6, 7], pulse-timing control [8], and coherent control [9], etc. These strategies are known to work when the system to be controlled is rather simple or small. However, the system can be complex [10] when we deal with highly excited states in large molecules or mesoscopic devices driven by electro-magnetic fields. Such a “complex” system in the limit of strong chaos is modelled by a random matrix Hamiltonian with a time-dependent external field [11], and the dynamics is well represented by multi-level-multi-level transitions with random interactions among energy levels. Although there are many works on the statistical properties [12, 13, 14, 15, 16] as well as the semiclassical properties [17, 18, 19] of eigenvalues under the variation of an external parameter, few works have been published on the dynamical properties of such systems except several studies on nonadiabatic processes [20, 21].

Even for such complex systems, there exist mathematical results showing complete controllability [22, 23] of general quantum systems with discrete spectrum under certain conditions. The existence of an optimal field is proved by optimal control theory (OCT) [24], which is a powerful tool to obtain an optimal field and has been studied for various dynamical systems [25, 26]. For the purpose of steering quantum states, many numerical schemes with monotonically convergent algorithms

[1, 27, 28] have been developed based on OCT. In general, OCT for quantum states provides sets of nonlinear differential equations (OCT equations) which are solved by iterative procedures. For complex systems with many degrees of freedom, however, the optimal field often becomes too complicated to analyze the dynamical processes involved. In addition, the computational cost becomes significantly heavy when we apply OCT to realistic problems with many degrees of freedom. Analytic approaches can be a good strategy to complement this annoying situation.

One such analytic method for multi-level control problems is STIRAP [5, 6, 7]. Though it can accomplish perfect control, it assumes an intermediate state coupled to initial and target states, and uses a pair of external fields with slowly varying amplitudes. Recently, we have proposed another analytic optimal field [29, 30] which induces a “direct” transition between random vectors in a random matrix system. The key idea of this approach is to describe the optimally controlled dynamics as a Rabi-like oscillation [2], and our optimal field can be interpreted as a generalized  $\pi$ -pulse [29]. Though the derivation and applicability of our analytic optimal field have been detailed in [30], there exists deficiency in our previous formula because of several (unnecessary) assumptions for simplification. In this paper, we rederive an analytic optimal field with less numbers of assumptions and reexamine its applicability to random matrix systems.

This paper is organized as follows. In Sec. II, we numerically investigate the multi-state control problem by OCT to show that, in some cases, the optimal field induces a smooth transition. According to this observation, in section III, we introduce a Rabi-like representation of the controlled state with some modifications compared to our previous result [29, 30]. Employing this representation, we obtain a new analytic expression of the optimal field. In Sec. III E, we confirm the applicability of the analytic field through the numerical integration of the Schrödinger’s equation for random matrix systems. Fi-

---

\*Present Address: Institut für Physikalische und Theoretische Chemie, J. W. Goethe-Universität, Max-von-Laue-Str. 7, D-60438 Frankfurt am Main, Germany

nally, in Sec. IV, we summarize this paper and give some discussions on the control problem of quantum chaos systems. We mention some technical details in Appendix.

## II. OPTIMAL CONTROL IN RANDOM MATRIX SYSTEMS

We present numerical results of controlled dynamics driven by an optimal field to see what kinds of dynamics are involved in random matrix systems. The random matrix Hamiltonian driven by a time-dependent external field  $\varepsilon(t)$  is written as

$$H[\varepsilon(t)] = H_0 + \varepsilon(t)V, \quad (1)$$

where  $H_0$  and  $V$  are random matrices subject to a certain universality class [11], i.e. Gaussian Orthogonal Ensemble (GOE), Gaussian Unitary Ensemble (GUE), etc.

It is well known that a strongly chaotic system does not have any constant of motion except the total energy [10], where the typical quantum states are random vectors. Thus, it is appropriate to choose initial and target states as random vectors. If we choose a certain ortho-normalized basis, a random vector in  $N$ -dimensional Hilbert space is represented by a set of random complex numbers  $\{c_j\}$ . If such a vector has neither special symmetry nor correlation, only the constraint imposed is the normalization condition,

$$\sum_{j=1}^N |c_j|^2 = 1. \quad (2)$$

where  $T$  and  $\alpha$  are given parameters representing the target time and the penalty factor, respectively. The quantum state  $|\phi(t)\rangle$  satisfies the initial condition,  $|\phi(0)\rangle = |\Phi_0\rangle$ . The first term in the right-hand side is the final overlap,

$$J_0 = |\langle\phi(T)|\Phi_T\rangle|^2. \quad (5)$$

The second term is the penalty term which minimizes the amplitude of the optimal field. In the third term, a Lagrange multiplier  $|\chi(t)\rangle$  is introduced to give a constraint that  $|\phi(t)\rangle$  satisfies Schrödinger's equation,

$$i\hbar \frac{d}{dt} |\phi(t)\rangle = H[\varepsilon(t)] |\phi(t)\rangle. \quad (6)$$

On the other hand, Schrödinger's equation for  $|\chi(t)\rangle$  is

$$i\hbar \frac{d}{dt} |\chi(t)\rangle = H[\varepsilon(t)] |\chi(t)\rangle, \quad (7)$$

Then, the normalized probability density for a variable  $y = |c_j|^2$  is given by

$$P_N(y) dy = N \exp(-Ny) dy, \quad (3)$$

when  $N$  is sufficiently large [11].

The actual procedure to numerically obtain an optimal field is as follows: The Hamiltonian (1) is constructed by generating two random matrices,  $H_0$  and  $V$ , with  $N \times N$  elements, where the scales of them are determined so that the averaged eigenvalue-spacing  $\Delta E$  of  $H_0$  and the variance  $\Delta V$  of off-diagonal elements of  $V$  are both unity. Next, we define an initial state  $|\Phi_0\rangle$  and a target state  $|\Phi_T\rangle$  as random vectors satisfying the distribution (3). Then, for a fixed target time  $T$ , the optimal field  $\varepsilon(t)$  is obtained by solving the OCT equations which are detailed in Sec. II A.

### A. Zhu-Botina-Rabitz Scheme of OCT

There are many effective methods to solve OCT equations for quantum systems [1]. In this section, we use a method introduced by Zhu, Botina, and Rabitz [27] (ZBR-OCT). Our goal is to determine the optimal external field  $\varepsilon(t)$  by which a given initial state  $|\Phi_0\rangle$  is steered to a given target state  $|\Phi_T\rangle$  at a target time  $T$ . According to ZBR-OCT, we introduce a functional  $J(\varepsilon(t), |\phi(t)\rangle)$

$$J(\varepsilon(t), |\phi(t)\rangle) = J_0 - \alpha \int_0^T [\varepsilon(t)]^2 dt - 2\text{Re} \left[ \langle\phi(T)|\Phi_T\rangle \int_0^T \langle\chi(t)| \frac{\partial}{\partial t} - \frac{H[\varepsilon(t)]}{i\hbar} |\phi(t)\rangle dt \right], \quad (4)$$

and the boundary condition  $|\chi(T)\rangle = |\Phi_T\rangle$  are obtained by “differentiating” the functional with respect to  $|\phi(t)\rangle$  and  $|\phi(T)\rangle$ . For the Hamiltonian (1), the variation of  $J$  with respect to  $\varepsilon(t)$  gives an expression for the optimal field,

$$\varepsilon(t) = \frac{1}{\alpha\hbar} \text{Im} [\langle\phi(t)|\chi(t)\rangle \langle\chi(t)|V|\phi(t)\rangle]. \quad (8)$$

This is a self-consistent expression for the optimal field, and to obtain its actual value, we have to simultaneously solve the nonlinear coupled equations, (6), (7) and (8) (OCT equations). ZBR-OCT is one such method which numerically solves the OCT equations with iterative procedures [27].

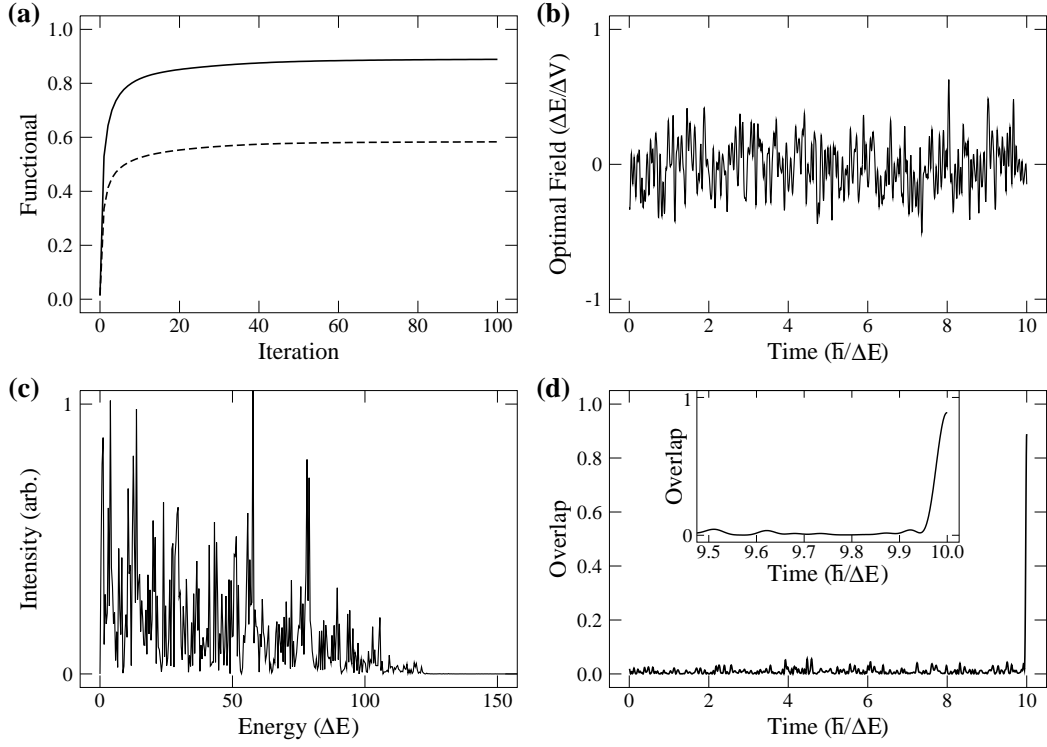


FIG. 1: Numerical results of controlled dynamics between random vectors in a  $128 \times 128$  GOE random matrix system. The optimal field is obtained through the iterative procedure given by Zhu, Botina, and Rabitz [27] for the target time  $T = 10$  and the penalty factor  $\alpha = 1$ . (a) Convergence property of functional values,  $J_0$  (solid curve) and  $J$  (dashed curve), as a function of the iteration step. (b) Optimal external field  $\varepsilon(t)$ . (c) Power spectrum of  $\varepsilon(t)$ . (d) Time evolution of the overlap  $|\langle \Phi_T | \psi(t) \rangle|^2$  (the magnified curve near  $t = T$  is shown in the inset).

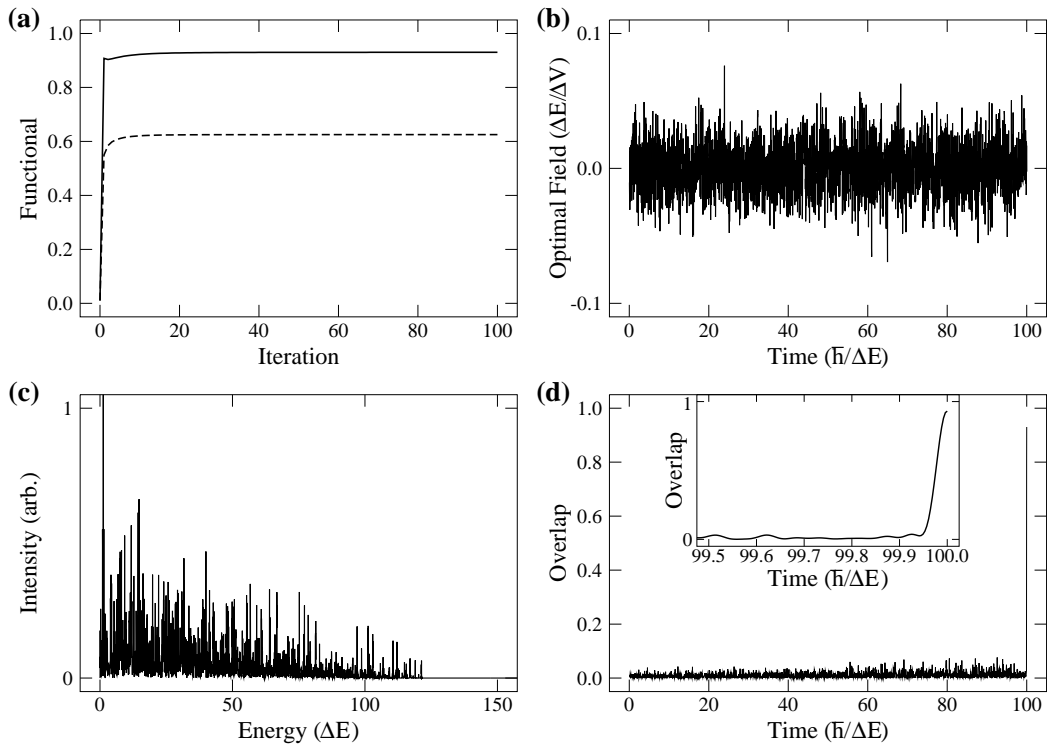


FIG. 2: The same as Fig. 1 except that the target time is longer ( $T = 100$ ) and the penalty factor is larger ( $\alpha = 10$ ).

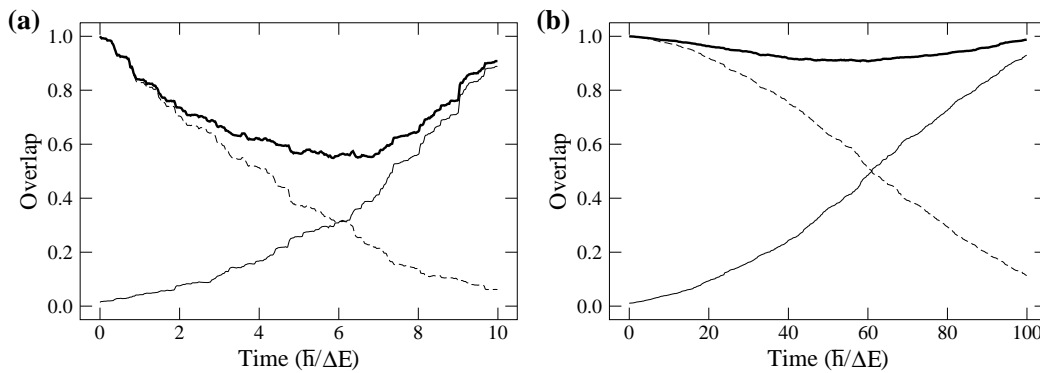


FIG. 3: Time evolution of the overlaps  $\langle \hat{P}_\chi(t) \rangle$  (solid curve),  $\langle \hat{P}_\phi(t) \rangle$  (dashed curve), and  $\langle \hat{P}_{\phi+\chi}(t) \rangle$  (thick curve) defined by Eqs. (11), (12) and (14). (a) and (b) correspond to Fig. 1 ( $T = 10$  and  $\alpha = 1$ ) and Fig. 2 ( $T = 100$  and  $\alpha = 10$ ), respectively.

## B. Numerical Results

We show controlled dynamics driven by numerically obtained optimal fields for a  $128 \times 128$  GOE random matrix Hamiltonian. The quantum state  $|\psi(t)\rangle$  with the initial condition  $|\psi(0)\rangle = |\Phi_0\rangle$  evolves according to Schrödinger's equation (6). We have chosen  $H_0$  and  $V$  so that  $\Delta E = \Delta V = 1$ . In other words, the energy values are shown in unit of  $\Delta E$ , and the unit of time is  $\hbar/\Delta E$ . Then, the field strength  $\varepsilon(t)$  is shown in unit of  $\Delta E/\Delta V$ .

In Fig. 1, we show the result with the parameters  $T = 10$  and  $\alpha = 1$ . The target time  $T = 10$  is comparable to the minimum time  $\tau_0 \approx 2\pi (\hbar/\Delta E)$  which is necessary to resolve each energy level from its adjacent levels. In Fig. 1(a), the functional values  $J_0$  (5) and  $J$  (4) are shown as the solid and dashed curves, respectively. They appear to converge after several ten steps. The final overlap  $J_0$  is 0.89 after 100 iterations. The optimal field  $\varepsilon(t)$  is shown in Fig. 1(b) as well as its Fourier spectrum in Fig. 1(c). Figure 1(d) shows the time evolution of the overlap  $|\langle \Phi_T | \psi(t) \rangle|^2$  with its magnification near the target time in the inset.

Figure 2 shows the result obtained for the parameters  $T = 100$  and  $\alpha = 10$ , which is the case of a relatively long target time compared to  $\tau_0$ . The values of  $J_0$  and  $J$ , the optimal field  $\varepsilon(t)$ , its Fourier spectrum, and the overlap  $|\langle \Phi_T | \psi(t) \rangle|^2$  are shown as in Fig. 1. In this calculation, the final overlap  $J_0$  is 0.93 after 100 iterations.

In both cases, the overlap  $|\langle \Phi_T | \psi(t) \rangle|^2$  as a function of time  $t$  remains small until  $t$  is close to the target time  $T$ . In multi-state quantum dynamics, even if no external field is applied, an auto-correlation function  $\langle \psi(0) | \psi(t) \rangle$  can rapidly decay by dephasing among dynamical phases of  $H_0$ . This is the reason why the overlaps  $\langle \Phi_T | \psi(t) \rangle$  in Fig. 1(d) and Fig. 2(d) rapidly grow up to the final values near  $t = T$ . In other words,  $\langle \Phi_T | \psi(t) \rangle$  decays quickly when  $t$  deviates from  $T$ .

## C. Observation of Smooth Transitions

Since we want to concentrate on transitions induced by  $\varepsilon(t)$  only, it is necessary to remove the contribution from dephasing by  $H_0$ . This is nothing but the procedure of the interaction picture in quantum mechanics [31]. We define time-dependent quantum states related to  $|\Phi_0\rangle$  and  $|\Phi_T\rangle$  by

$$|\phi_0(t)\rangle = \hat{U}_0(t, 0)|\Phi_0\rangle, \quad |\chi_0(t)\rangle = \hat{U}_0(t, T)|\Phi_T\rangle, \quad (9)$$

where  $\hat{U}_0(t_2, t_1)$  represents a propagator from  $t = t_1$  to  $t = t_2$  with respect to the unperturbed Hamiltonian  $H_0$ . We call these states “moving bases.” In the following, we analyze the optimally controlled dynamics through these time-dependent states.

If we introduce projection operators associated with these states by

$$\hat{P}_\phi(t) = |\phi_0(t)\rangle\langle\phi_0(t)|, \quad \hat{P}_\chi(t) = |\chi_0(t)\rangle\langle\chi_0(t)|, \quad (10)$$

the probabilities such that  $|\psi(t)\rangle$  is found in these states are written as

$$\langle \hat{P}_\phi(t) \rangle \equiv \langle \psi(t) | \hat{P}_\phi | \psi(t) \rangle, \quad (11)$$

$$\langle \hat{P}_\chi(t) \rangle \equiv \langle \psi(t) | \hat{P}_\chi | \psi(t) \rangle. \quad (12)$$

These values are more appropriate quantities to observe the multi-level-multi-level transition dynamics compared to the bare overlap  $|\langle \Phi_T | \psi(t) \rangle|^2$  as shown below. In addition, we introduce another projection operator

$$\hat{P}_{\phi+\chi}(t) = \frac{\hat{P}_\phi(t) + \hat{P}_\chi(t) - \hat{P}_\phi(t)\hat{P}_\chi(t) - \hat{P}_\chi(t)\hat{P}_\phi(t)}{1 - \text{tr}[\hat{P}_\chi(t)\hat{P}_\phi(t)]}, \quad (13)$$

which represents projection onto a subspace defined by a linear superposition of  $|\phi_0(t)\rangle$  and  $|\chi_0(t)\rangle$ . We can prove that this is a projection operator by using  $1 - \text{tr}[\hat{P}_\phi(t)\hat{P}_\chi(t)] = 1 - |\langle \phi_0 | \chi_0 \rangle|^2$  and  $\hat{P}_\phi(t)\hat{P}_\chi(t)\hat{P}_\phi(t) = |\langle \phi_0 | \chi_0 \rangle|^2 \hat{P}_\phi(t)$ , etc. Then, the quantity,

$$\langle \hat{P}_{\phi+\chi}(t) \rangle \equiv \langle \psi(t) | \hat{P}_{\phi+\chi}(t) | \psi(t) \rangle, \quad (14)$$

represents the probability that the quantum state  $|\psi(t)\rangle$  is found on the subspace.

In Fig. 3(a) and (b), we show the overlaps (probabilities),  $\langle \hat{P}_\phi(t) \rangle$ ,  $\langle \hat{P}_\chi(t) \rangle$ , and  $\langle \hat{P}_{\phi+\chi}(t) \rangle$ , calculated from the results in Figs. 1 and 2. All the curves in Fig. 3(b) are smoother than those in Fig. 3(a). It is also worth noting that  $\langle \hat{P}_{\phi+\chi}(t) \rangle$  stays close to unity for all the time in Fig. 3(b).

From other ZBR-OCT calculations for random matrix systems, we found that the ZBR optimal field induces a transition from  $|\Phi_0\rangle$  to  $|\Phi_T\rangle$  nearly within a subspace spanned by  $|\phi_0(t)\rangle$  and  $|\chi_0(t)\rangle$  when the target time  $T$  is sufficiently large. Based on this finding, we will develop an analytic approach for the optimal field in the next section.

### III. ANALYTIC APPROACH FOR CONTROLLED DYNAMICS

The Rabi oscillation in a two-level system has been studied in detail [2]. According to such previous works, we can represent a wavefunction as a linear combination of two eigenstates  $|\varphi_1\rangle$  and  $|\varphi_2\rangle$  with eigen-energies  $E_1$  and  $E_2$ ,

$$|\psi(t)\rangle = A(t)|\varphi_1\rangle e^{E_1 t/i\hbar} + B(t)|\varphi_2\rangle e^{E_2 t/i\hbar}. \quad (15)$$

Here the coefficients  $A(t)$  and  $B(t)$  are slowly oscillating functions with a Rabi frequency under the rotating-wave approximation (RWA) [2].

In this section, we show, under certain conditions, that a Rabi-like description becomes valid even for multi-level quantum systems where the wavefunction is described by the time-dependent states in Eq. (9). We call these states ‘‘moving bases’’ instead of eigenstates. This is equivalent to considering the case where the controlled state remains in the subspace spanned by these moving bases over a whole period of the dynamics. With the help of OCT, we conversely obtain an analytical expression for the optimal field to induce the smooth transition we found in Fig. 3 for the multi-level dynamics.

#### A. Rabi-like Representation

In the previous section, we have defined the moving bases  $|\phi_0(t)\rangle$  and  $|\chi_0(t)\rangle$  (9) in order to observe smooth transitions in OCT calculations. Unlike the two-level case, however, these states are not always orthogonal to each other. The inner-product between them is written in the form,

$$\langle \phi_0(t) | \chi_0(t) \rangle = \langle \Phi_0 | \hat{U}(0, T) | \Phi_T \rangle = i e^{i\theta} \sin \Theta, \quad (16)$$

with  $0 \leq \Theta \leq \pi/2$  and  $0 \leq \theta < 2\pi$ . Note that the inner-product (16) does not depend on  $t$ , i.e. constant in time, despite that the moving bases ( $|\phi_0(t)\rangle$  and  $|\chi_0(t)\rangle$ ) rapidly change their ‘‘directions’’ according to the Schrödinger’s equations.

In our previous works [29, 30], we have used an assumption that  $\Theta = 0$ . Actually we can remove this assumption by introducing an orthogonal pair of the moving bases as (Schmidt decomposition)

$$|\tilde{\phi}_0(t)\rangle = |\phi_0(t)\rangle, \quad (17)$$

$$|\tilde{\chi}_0(t)\rangle = \frac{|\chi_0(t)\rangle - i e^{i\theta} \sin \Theta |\phi_0(t)\rangle}{\cos \Theta}. \quad (18)$$

These are our new moving bases which are orthogonal to each other and will be used below.

We introduce a Rabi-like representation of the quantum state  $|\phi(t)\rangle$  with an initial condition  $|\phi(0)\rangle = |\Phi_0\rangle$  by a linear combination of the new moving bases  $|\tilde{\phi}_0(t)\rangle$  and  $|\tilde{\chi}_0(t)\rangle$ ,

$$|\phi(t)\rangle = A(t)|\tilde{\phi}_0(t)\rangle + B(t)|\tilde{\chi}_0(t)\rangle. \quad (19)$$

The coefficients,  $A(t)$  and  $B(t)$ , must satisfy a normalization condition,

$$|A(t)|^2 + |B(t)|^2 = 1. \quad (20)$$

If this representation is valid,  $A(t)$  and  $B(t)$  satisfy the following differential equations,

$$\frac{d}{dt} A(t) = \frac{\varepsilon(t)}{i\hbar} \left[ \langle \tilde{\phi}_0(t) | V | \tilde{\phi}_0(t) \rangle A(t) + \langle \tilde{\phi}_0(t) | V | \tilde{\chi}_0(t) \rangle B(t) \right], \quad (21)$$

$$\frac{d}{dt} B(t) = \frac{\varepsilon(t)}{i\hbar} \left[ \langle \tilde{\chi}_0(t) | V | \tilde{\phi}_0(t) \rangle A(t) + \langle \tilde{\chi}_0(t) | V | \tilde{\chi}_0(t) \rangle B(t) \right]. \quad (22)$$

#### B. Rotating Wave Approximation

The rotating-wave approximation (RWA) means dropping rapidly oscillating terms in differential equations [2]. Since RWA is applicable to non-degenerate multi-level

systems [6], we will apply RWA to Eqs. (21) and (22) to solve them approximately.

To justify the use of RWA, we introduce three integrals,

$$I_\Omega(t) = \frac{1}{\hbar} \int_0^t \varepsilon(t') \langle \tilde{\phi}_0(t') | V | \tilde{\chi}_0(t') \rangle dt', \quad (23)$$

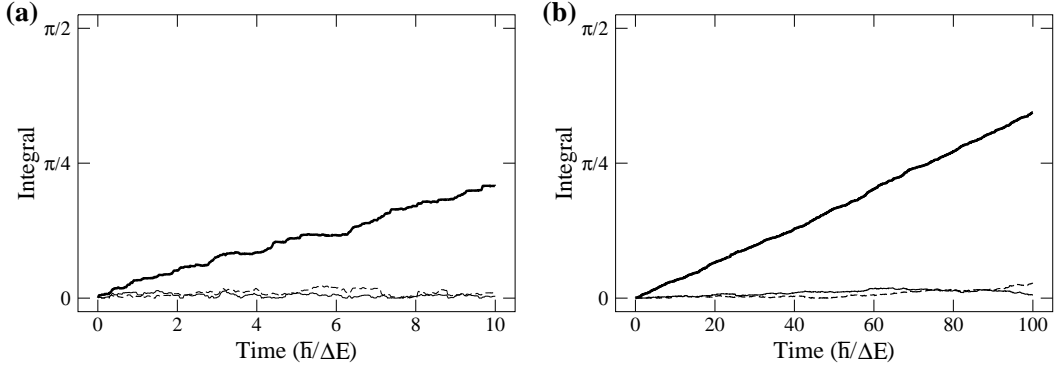


FIG. 4: Time evolution of  $|I_\Omega(t)|$  (thick line),  $|I_\phi(t)|$  (solid line), and  $|I_\chi(t)|$  (dashed line), defined by Eqs. (23), (24), and (25), respectively. (a) and (b) correspond to Fig. 1 ( $T = 10$  and  $\alpha = 1$ ) and Fig. 2 ( $T = 100$  and  $\alpha = 10$ ), respectively.

$$I_\phi(t) = \frac{1}{\hbar} \int_0^t \varepsilon(t') \langle \tilde{\phi}_0(t') | V | \tilde{\phi}_0(t') \rangle dt', \quad (24)$$

$$I_\chi(t) = \frac{1}{\hbar} \int_0^t \varepsilon(t') \langle \tilde{\chi}_0(t') | V | \tilde{\chi}_0(t') \rangle dt'. \quad (25)$$

Note that the generalized pulse area [29] is represented by  $2|I_\Omega(T)|$ . The numerical results in Figs. 1 and 2 are used to calculate these integrals explicitly, and their absolute values are plotted in Fig. 4. Since  $I_\phi(t)$  and  $I_\chi(t)$  are almost zero, it is appropriate to assume that

$$I_\phi(t) = I_\chi(t) = 0, \quad (26)$$

which corresponds to RWA. Furthermore, for a long target time, we can employ the following form

$$I_\Omega(t) = \Omega t, \quad (27)$$

which means that, with use of RWA, the integrand in Eq. (23) is nearly constant in time.

Under these approximations (26) and (27), the differential equations, (21) and (22), are simplified to

$$\frac{d}{dt} A(T) = -i\Omega B(t), \quad \frac{d}{dt} B(T) = -i\Omega^* A(t). \quad (28)$$

For the initial value problem with the conditions,  $A(0) = 1$  and  $B(0) = 0$ , we obtain a solution,

$$A(t) = \cos[|\Omega|t], \quad B(t) = -\frac{i|\Omega|}{\Omega} \sin[|\Omega|t]. \quad (29)$$

Defining the phase of  $\Omega$  as

$$\frac{\Omega}{|\Omega|} = e^{i\theta}, \quad (30)$$

we finally obtain

$$|\phi(t)\rangle = |\tilde{\phi}_0(t)\rangle \cos[|\Omega|t] - ie^{-i\theta} |\tilde{\chi}_0(t)\rangle \sin[|\Omega|t] = \frac{\cos[|\Omega|t + \theta]}{\cos \theta} |\phi_0(t)\rangle - \frac{ie^{-i\theta} \sin[|\Omega|t]}{\cos \theta} |\chi_0(t)\rangle. \quad (31)$$

This state oscillates with the frequency  $|\Omega|$  between  $|\tilde{\phi}_0(t)\rangle$  and  $|\tilde{\chi}_0(t)\rangle$ , as well as between  $|\phi_0(t)\rangle$  and  $|\chi_0(t)\rangle$ .

### C. Analytic Field

According to the ZBR-OCT scheme in Sec. II A, the optimal external field is represented by Eq. (8) given the forward evolving state  $|\phi(t)\rangle$  and the backward evolving state  $|\chi(t)\rangle$  are prepared with the boundary conditions,

$$|\phi(0)\rangle = |\Phi_0\rangle, \quad |\chi(T)\rangle = |\Phi_T\rangle. \quad (32)$$

Under the approximations (26) and (27),  $|\phi(t)\rangle$  has been already given in Eq. (31), and  $|\chi(t)\rangle$  is written as

$$|\chi(t)\rangle = -ie^{i\theta} |\tilde{\phi}_0(t)\rangle \sin[|\Omega|(t-T) - \theta] + |\tilde{\chi}_0(t)\rangle \cos[|\Omega|(t-T) - \theta] \quad (33)$$

$$= -\frac{ie^{i\theta} \sin[|\Omega|(t-T)]}{\cos \theta} |\phi_0(t)\rangle + \frac{\cos[|\Omega|(t-T) - \theta]}{\cos \theta} |\chi_0(t)\rangle. \quad (34)$$

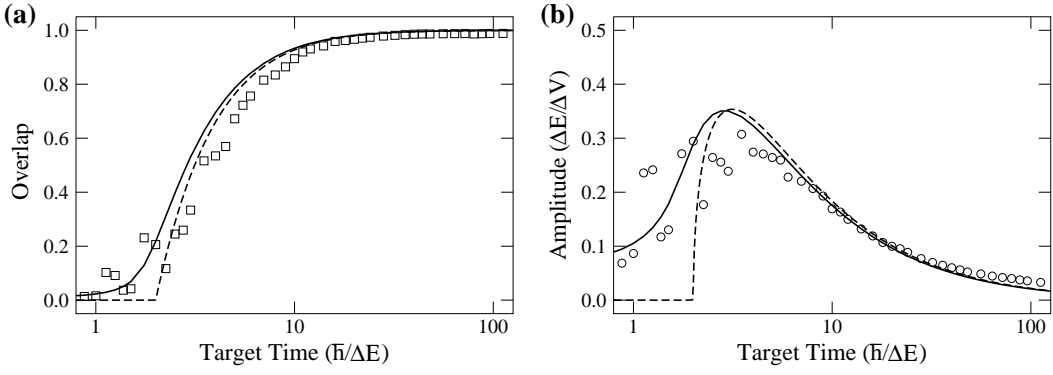


FIG. 5: Numerical results (squares and circles) by OCT with the penalty factor  $\alpha = 1$  are compared to our theoretical values: (a) Final overlap  $J_0$ . (b) Averaged amplitude  $\bar{\varepsilon}$  of the external field. The solid (dashed) curve corresponds to the case of  $\sin \Theta = \sqrt{\pi/4N}$  ( $\Theta = 0$ ).

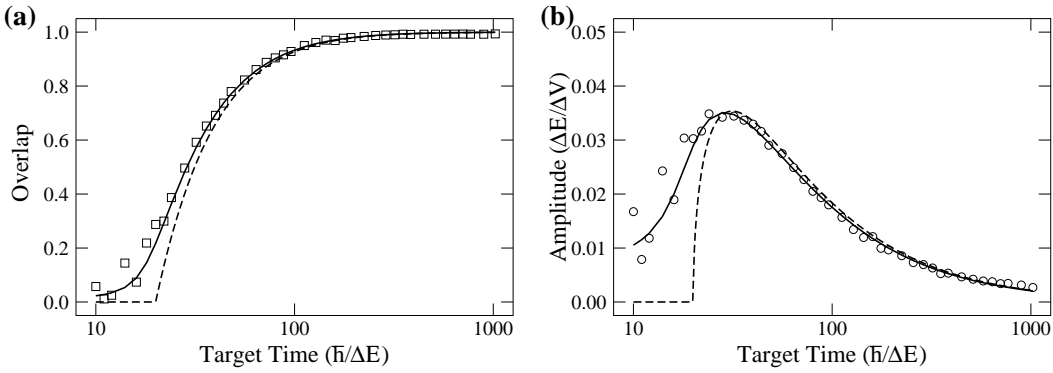


FIG. 6: The same as Fig. 5 except that the penalty factor is larger ( $\alpha = 10$ ).

The overlap between these states is

$$\langle \phi(t) | \chi(t) \rangle = i e^{i\theta} \sin[|\Omega|T + \Theta]. \quad (35)$$

Substituting Eqs. (31) and (33) into  $|\phi(t)\rangle$  and  $|\chi(t)\rangle$  in Eq. (8), we obtain the external field,

$$\varepsilon(t) = \frac{\sin[2(|\Omega|T + \Theta)]}{2\alpha\hbar} \text{Re} \left[ e^{i\theta} \langle \tilde{\chi}_0(t) | V | \tilde{\phi}_0(t) \rangle \right]. \quad (36)$$

By calculating  $I_\Omega(T)$  for the external field (36) and using Eq. (27) at  $t = T$ , we obtain an equation for  $\Omega$ ,

$$\Omega = \frac{\sin[2(|\Omega|T + \Theta)]}{4\alpha\hbar^2} [e^{i\theta} \bar{V}^2 + e^{-i\theta} \bar{W}^2] \quad (37)$$

where  $\bar{V}^2$  and  $\bar{W}^2$  are defined by averages of transition elements,

$$\bar{V}^2 = \frac{1}{T} \int_0^T |\langle \tilde{\phi}_0(t) | V | \tilde{\chi}(t) \rangle|^2 dt, \quad (38)$$

$$\bar{W}^2 = \frac{1}{T} \int_0^T [\langle \tilde{\phi}_0(t) | V | \tilde{\chi}(t) \rangle]^2 dt. \quad (39)$$

Note that  $|\bar{W}^2|$  becomes small compared to  $\bar{V}^2$  when the system is sufficiently large without special symmetry (see

Eqs. (A20) and (A21)). Then, we obtain an equation for  $|\Omega|$  with use of Eq. (30),

$$|\Omega| = \frac{\bar{V}^2 \sin[2(|\Omega|T + \Theta)]}{4\alpha\hbar^2}. \quad (40)$$

The solutions of this equation are obtained from the crossing points between  $y = x/T$  and  $y = (K/2) \sin[2(x + \Theta)]$  where  $x \equiv |\Omega|T$  and  $K \equiv \bar{V}^2/(2\alpha\hbar^2)$ .

To illustrate the effectiveness of our result, we calculate the final overlap  $J_0$  from Eq. (35)

$$J_0 = |\langle \phi(t) | \chi(t) \rangle|^2 = \sin^2[|\Omega|T + \Theta] \quad (41)$$

and the average amplitude of the optimal field from Eq. (36)

$$\bar{\varepsilon} = \sqrt{\frac{1}{T} \int_0^T |\varepsilon(t)|^2 dt} \simeq \frac{\sqrt{2}\hbar|\Omega|}{V}. \quad (42)$$

These estimates match well with the numerical results (squares and circles) as shown in Figs. 5 and 6. Since the inner product between  $N$  dimensional random complex vectors is  $\sim \sqrt{\pi/4N}$  as an average (see Eq. (A19)),

we have used  $|\langle\phi_0(t)|\chi_0(t)\rangle| = \sin\Theta \simeq \sqrt{\pi/4N}$  (solid lines). For comparison, we also show the results for  $\Theta = 0$  (dashed lines), which correspond to our previous results [29, 30]. It is obvious that the new analytic field outperforms the previous one.

#### D. Perfect Control

In the ZBR-OCT scheme (Sec. II A), we need a finite value of the penalty factor  $\alpha$  in order to avoid numerical instability. In the analytic approach, however, the limit  $\alpha \rightarrow 0$  can be taken safely in Eq. (40). In this case, the solution of Eq. (40) becomes

$$|\Omega\rangle \rightarrow \Omega_m = \frac{1}{T} \left( \frac{\pi}{2} - \Theta + m\pi \right), \quad (43)$$

where  $m$  is an integer. It is easily shown that this gives  $J_0 = 1$  from Eq. (41). From Eqs. (36) and (40), the external field is obtained as

$$\varepsilon(t) = \frac{2\hbar\Omega_m}{V^2} \text{Re} \left[ e^{i\theta} \langle\tilde{\chi}_0(t)|V|\tilde{\phi}_0(t)\rangle \right]. \quad (44)$$

Since this equation does not contain  $\alpha$ , it is different from other non-iterative optimal fields [32]. It can be shown that this field actually achieves perfect control in the limit of  $T$ ,  $N \rightarrow \infty$ . We give the proof in Appendix A 4.

#### E. Application of the Analytic Field

Although it is theoretically exact for  $T$ ,  $N \rightarrow \infty$ , our approach is applicable to the cases with finite  $T$  and  $N$  as already given in Figs. 5 and 6.

In Fig. 7, we show time evolutions of the overlaps with  $T = 10$  (a) and  $T = 100$  (b). The initial and target states are the same as in Fig. 3. Unlike the results by OCT (Fig. 3), the probability on the subspace spanned by  $|\phi_0(t)\rangle$  and  $|\chi_0(t)\rangle$  decreases monotonically. This is because the analytic field (44) was obtained under the conditions  $T$ ,  $N \rightarrow \infty$  while the numerical calculations were performed for finite  $T$  and  $N$ .

The performance of the analytic optimal field can be easily seen by plotting the final overlap  $J_0$  for various values of  $N$  and  $T$  (Fig. 8). The errorbars in this figure represent the normal deviation of  $J_0$  obtained from calculations for 100 different samples of the Hamiltonian and state vector. By comparing with our previous result, Fig. 1 in [29], our new analytic field outperforms the previous one for the intermediate  $T$  and  $N$  as expected. This is a nice feature when we consider the application of this method to non-limiting cases.

## IV. SUMMARY AND DISCUSSION

In this paper, we have proposed an analytic approach for controlling quantum states in random matrix systems.

From the analysis of OCT calculations, we showed that optimally controlled states remain on a subspace spanned by two “moving bases” when the target time and system size are both sufficiently large. According to this observation, we developed a new method to solve OCT equations and to obtain an analytic expression for the optimal field. Finally, it was numerically shown that the analytic field actually steers the quantum states in random matrix systems. The difference from our previous result is that we have taken new moving bases which are exactly orthogonal, and the newly obtained analytic field outperforms the previous one for the intermediate target time and system size.

Our analytic field (44) is a generalized  $\pi$ -pulse [29] in multi-level systems, which is realized because of certain randomness in the elements of the Hamiltonian and state vectors. The amplitude of the pulse becomes smaller when the target time  $T$  is larger since an effective pulse area should be a constant  $\pi$  [29]. Although our controlled dynamics seems to be antithetical to the molecular processes induced by intense laser fields [33, 34], this does not necessarily mean that our approach is not applicable to those systems. This is because such dynamics driven by the intense laser field can be included in the “unperturbed” Hamiltonian  $H_0$ . If the system becomes strongly chaotic by the laser field, such a situation is even preferable for the prerequisite of our approach using random matrix Hamiltonians.

The quantum targeting problem studied in this paper was solved analytically for random matrix systems, while it is known that classical targeting problems [35, 36] are difficult to be solved for strongly chaotic cases. This is because there is sensitivity of trajectories with respect to initial values. Our result for quantum systems thus seems to break the naive quantum-classical correspondence. It is important to clarify how the correspondence is recovered in the semiclassical limit [37, 38].

Recently Gong and Brumer showed that coherent control works for a quantized kicked rotor [39, 40], a typical “quantum chaos” system, whereas our concern was optimal control of quantum states in random matrix systems. Optimal control for quantum chaos systems, especially weakly chaotic systems, is another interesting subject which should be pursued [30, 41].

#### Acknowledgements

The authors thank Prof. S.A. Rice, Prof. H. Rabitz, Prof. M. Toda, Prof. H. Nakamura, Prof. H. Kono, Prof. S. Tasaki, Prof. A. Shudo, Dr. Y. Ohtsuki, and Dr. G.V. Mil’nikov for useful discussions.



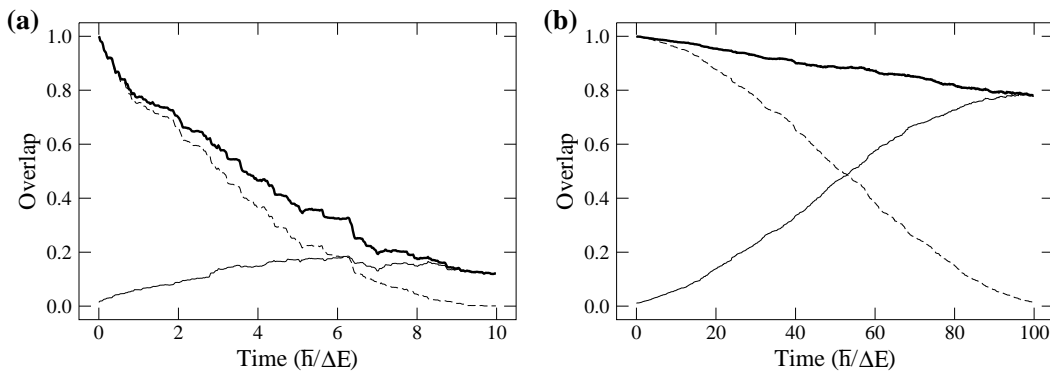


FIG. 7: The same as Fig. 3 except that we have used the analytic optimal field Eq. (44). (a) and (b) correspond to  $T = 10$  and  $T = 100$ , respectively.

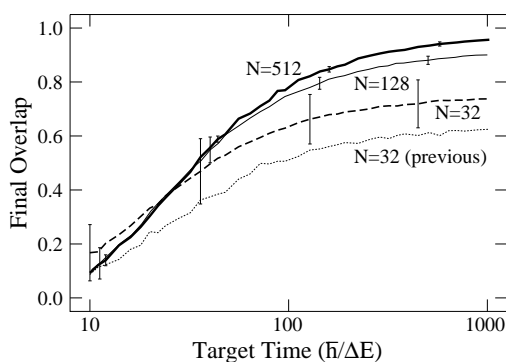


FIG. 8: The final overlap  $J_0$  obtained by the analytic optimal field. We show the results for various system sizes according to the following procedure: At first, we generate two random matrices ( $H_0$  and  $V$ ) and two random vectors ( $|\Phi_0\rangle$  and  $|\Phi_T\rangle$ ) for a system size  $N$ . If we choose a target time  $T$ , the analytic field is given by Eq. (44). The quantum state  $|\psi(t)\rangle$  at  $t = T$  is obtained by numerical integration of Schrödinger's equation under the field with the initial condition  $|\psi(0)\rangle = |\Phi_0\rangle$ . Finally, the final overlap  $J_0$  is calculated by  $|\langle\Phi_T|\psi(T)\rangle|^2$ . Each curve in the figure is obtained as an ensemble average over 100 different realizations of random numbers. Compare this with Fig. 1 in the previous study [29] (only the data of  $N = 32$  is shown as a dotted curve in this figure for comparison).

## APPENDIX A: EIGENSTATE REPRESENTATION

### 1. Preliminary

Though our results in the main text do not depend on a particular representation, in this appendix, we describe the controlled dynamics and the analytic optimal field Eq. (44) by using the eigenstate representation of  $H_0$ , and prove that perfect control is achieved by Eq. (44).

We introduce eigenstates  $|\varphi_j\rangle$  of  $H_0$  corresponding to eigenvalues  $E_j$  where  $\{|\varphi_j\rangle\}$  constitute an orthonormal

basis set. The initial and target states

$$|\Phi_0\rangle = \sum_{j=1}^N c_j |\varphi_j\rangle, \quad |\Phi_T\rangle = \sum_{j=1}^N d_j |\varphi_j\rangle \quad (\text{A1})$$

are represented by random complex numbers  $\{c_j\}$  and  $\{d_j\}$  satisfying normalization conditions,

$$\sum_{j=1}^N |c_j|^2 = \sum_{j=1}^N |d_j|^2 = 1. \quad (\text{A2})$$

The matrix elements of  $V$  are defined by using  $\{|\varphi_j\rangle\}$

$$V_{jk} = \langle\varphi_j|V|\varphi_k\rangle. \quad (\text{A3})$$

These quantities,  $\{c_j\}$ ,  $\{d_j\}$  and  $\{V_{jk}\}$ , are assumed to be uncorrelated among them.

### 2. The Analytic Optimal Field

The moving bases, Eq. (9), satisfying  $|\phi(0)\rangle = |\Phi_0\rangle$  and  $|\chi(T)\rangle = |\Phi_T\rangle$  can be written as

$$|\phi_0(t)\rangle = \sum_{j=1}^N c_j |\varphi_j\rangle e^{E_j t / i\hbar}, \quad (\text{A4})$$

$$|\chi_0(t)\rangle = \sum_{j=1}^N d_j |\varphi_j\rangle e^{E_j (t-T) / i\hbar}, \quad (\text{A5})$$

where  $T$  represents the target time. In general, these states are not orthogonal to each other as shown in Eq. (16), and the orthogonal (new) moving bases, Eqs. (17) and (18), are constructed as

$$|\tilde{\phi}_0(t)\rangle = \sum_{j=1}^N c_j |\varphi_j\rangle e^{E_j t / i\hbar}, \quad (\text{A6})$$

$$|\tilde{\chi}_0(t)\rangle = \sum_{j=1}^N \frac{d_j e^{-E_j T / i\hbar} - i e^{i\theta} c_j \sin \Theta}{\cos \Theta} |\varphi_j\rangle e^{E_j t / i\hbar}$$

$$\equiv \sum_{j=1}^N \tilde{d}_j |\varphi_j\rangle e^{E_j t / i\hbar}. \quad (\text{A7})$$

Substituting these states into Eq. (44), we obtain the eigenstate representation of the analytic optimal field,

$$\varepsilon(t) = \frac{2\hbar\Omega_m}{\bar{V}^2} \text{Re} \left[ e^{i\theta} \sum_{j=1}^N \sum_{k=1}^N \tilde{d}_j^* V_{jk} c_k \exp \left\{ \frac{(E_k - E_j)t}{i\hbar} \right\} \right]. \quad (\text{A8})$$

### 3. Sum of Random Variables

Suppose a probability variable  $Y$  is defined by a sum of independent probability variables  $X_j$  ( $j = 1, \dots, n$ ),

$$Y = X_1 + X_2 + \dots + X_n, \quad (\text{A9})$$

with an expectation  $\mathcal{M}(X_j) = \mathcal{M}_X$  ( $> 0$ ) and a variance  $\sigma^2(X_j) = \sigma_X^2$ . When  $n$  is sufficiently large, it is known from the central limit theorem that  $Y$  is normally distributed. The expectation and variance are

$$\mathcal{M}(Y) = n\mathcal{M}_X, \quad \sigma^2(Y) = n\sigma_X^2. \quad (\text{A10})$$

Then, the expectation  $n\mathcal{M}_X$  can be used as an approximate value of  $Y$  since the relative standard deviation

$$\sigma_{\text{rel}} \equiv \frac{\sqrt{\sigma^2(Y)}}{\mathcal{M}(Y)} = \frac{\sigma_X}{\mathcal{M}_X \sqrt{n}} \simeq O(1/\sqrt{n}) \quad (\text{A11})$$

vanishes for  $n \rightarrow \infty$ .

Using the above basic knowledge, we estimate approximated values for sums of  $V_{kj}$ ,  $c_j$ , and  $\tilde{d}_k$  in the following. The coefficients  $c_j$  and  $\tilde{d}_j$  are independent random numbers subject to the distribution function (3), i.e.,

$$\mathcal{M}(|c_j|^2) = \mathcal{M}(|\tilde{d}_j|^2) = \frac{1}{N}, \quad (\text{A12})$$

$$\sigma^2(|c_j|^2) = \sigma^2(|\tilde{d}_j|^2) = \frac{1}{N^2}. \quad (\text{A13})$$

For large  $N$ , we obtain

$$\begin{aligned} \sum_{j=1}^N |V_{kj}|^2 |c_j|^2 &\simeq N \mathcal{M}(|V_{kj}|^2 |c_j|^2) \\ &= \mathcal{M}(|V_{kj}|^2) + O(1/\sqrt{N}), \end{aligned} \quad (\text{A14})$$

$$\begin{aligned} \sum_{k=1}^N |\tilde{d}_k|^2 |V_{kj}|^2 &\simeq N \mathcal{M}(|\tilde{d}_k|^2 |V_{kj}|^2) \\ &= \mathcal{M}(|V_{kj}|^2) + O(1/\sqrt{N}), \end{aligned} \quad (\text{A15})$$

where we have used a basic relation

$$\mathcal{M}(X_1 X_2 \dots X_n) = \mathcal{M}(X_1) \mathcal{M}(X_2) \dots \mathcal{M}(X_n) \quad (\text{A16})$$

for independent probability variables  $X_j$ .

Applying the central limit theorem to a sum of complex variables  $Z_n = z_1 + z_2 + \dots + z_n \equiv X_n + iY_n$  with  $\mathcal{M}(z_j) = 0$  and  $\mathcal{M}(|z_j|^2) = \sigma_z^2$ , we have

$$\begin{aligned} P(X_n)P(Y_n) dX_n dY_n \\ = \frac{1}{\pi n \sigma_z^2} \exp \left( -\frac{X_n^2 + Y_n^2}{n \sigma_z^2} \right) dX_n dY_n. \end{aligned} \quad (\text{A17})$$

Then, the average magnitude of  $|Z_n|$  can be calculated as

$$\mathcal{M}(|Z_n|) = \int |Z_n| P(X_n) P(Y_n) dX_n dY_n = \frac{\sqrt{\pi n \sigma_z^2}}{2}. \quad (\text{A18})$$

From this relation, the inner product, Eq. (16), is estimated as

$$|\langle \phi_0(t) | \chi_0(t) \rangle| \simeq \frac{\sqrt{\pi N} \mathcal{M}(|c_j|^2 |d_j|^2)}{2} = \sqrt{\frac{\pi}{4N}}. \quad (\text{A19})$$

In the same manner, the average transition elements (38) and (39) are estimated as

---

in the limit  $T \rightarrow \infty$ . Thus, we can ignore  $\bar{W}^2$  for  $T, N \rightarrow \infty$ .

### 4. Controlled State

We give a proof that a quantum state driven by the analytic field, Eq. (44) or (A8), actually shows a smooth

---


$$\bar{V}^2 = \left| \sum_j c_j^* V_{jj} \tilde{d}_j \right|^2 + \sum_j \sum_{k \neq j} \left| c_j^* V_{jk} \tilde{d}_k \right|^2 \simeq \mathcal{M}(|V_{kj}|^2) + O(1/N), \quad (\text{A20})$$

$$\bar{W}^2 = \left( \sum_j c_j^* V_{jj} \tilde{d}_j \right)^2 + 2 \sum_j \sum_{k < j} c_j^* c_k^* |V_{jk}|^2 \tilde{d}_j \tilde{d}_k \simeq O(1/N), \quad (\text{A21})$$


---

transition between the initial and target states. We assume that the size  $N$  of the random matrix Hamiltonian  $H_0$  and the target time  $T$  are both large enough.

To see the dynamics induced by the field, we represent a quantum state in the eigenstate representation,

$$|\psi(t)\rangle = \sum_j a_j(t) |\varphi_j\rangle e^{E_j t / i\hbar}, \quad (\text{A22})$$

which satisfies the initial condition  $|\psi(0)\rangle = |\Phi_0\rangle$ . From the Schrödinger's equation driven by the optimal field (A8), we obtain the following differential equations for  $a_j(t)$ ,

$$\dot{a}_k(t) = -i \sum_{j \neq k} \Omega_{kj} a_j(t), \quad (\text{A23})$$

where  $\Omega_{kj}$  is defined by

$$\Omega_{kj} = \frac{\Omega_m |V_{kj}|^2}{\bar{V}^2} (c_j^* \tilde{d}_k + \tilde{d}_j^* c_k), \quad (\text{A24})$$

and we have used the rotating-wave approximation. We write  $a_k(t)$  in the following form,

$$a_k(t) = A_k \cos \Omega_m t + B_k \sin \Omega_m t, \quad (\text{A25})$$

and  $A_k$  and  $B_k$  are determined as

$$A_k = c_k, \quad B_k = -i \sum_{j \neq k} \frac{\Omega_{kj}}{\Omega_m} c_j, \quad (\text{A26})$$

from the initial conditions  $a_k(0) = c_k$  and (A23).

Using the relations (A14) and (A15), we obtain

$$\sum_{j \neq k} \frac{\Omega_{kj}}{\Omega_m} c_j = \tilde{d}_k \sum_{j \neq k} \frac{|V_{kj}|^2 |c_j|^2}{\bar{V}^2} + c_k \sum_{j \neq k} \frac{|V_{kj}|^2 c_j \tilde{d}_j^*}{\bar{V}^2} \simeq \tilde{d}_k + O(1/N), \quad (\text{A27})$$

$$\sum_{j \neq k} \frac{\Omega_{kj}}{\Omega_m} \tilde{d}_j = \tilde{d}_k \sum_{j \neq k} \frac{|V_{kj}|^2 c_j^* \tilde{d}_j}{\bar{V}^2} + c_k \sum_{j \neq k} \frac{|V_{kj}|^2 |\tilde{d}_k|^2}{\bar{V}^2} \simeq c_k + O(1/N). \quad (\text{A28})$$

Substituting (A27) into (A25), we obtain

$$a_k(t) = c_k \cos \Omega_m t - i \tilde{d}_k \sin \Omega_m t, \quad (\text{A29})$$

and the right-hand side of the differential equation (A23) becomes

$$-i \sum_{j \neq k} \Omega_{kj} a_j(t) = -\Omega_m (c_k \sin \Omega_m t + i \tilde{d}_k \cos \Omega_m t) \quad (\text{A30})$$

with use of (A27) and (A28). Since Eq. (A30) is exactly the same as  $\dot{a}_k(t)$ , we have confirmed that (A29) is the

solution for the Schrödinger's equation driven by the analytical optimal field.

The final expression (A29) shows that each  $a_k(t)$  smoothly changes its value from  $c_k$  at  $t = 0$  to  $\tilde{d}_k$  at  $t = T$  as expected, and the overlap between  $|\psi(t)\rangle$  and  $|\chi_0(t)\rangle$  is easily calculated as

$$\langle \chi_0(t) | \psi(t) \rangle = -i \sin \Omega_m t. \quad (\text{A31})$$

This shows  $|\langle \Phi_T | \psi(T) \rangle| = 1$ , i.e. perfect control is accomplished at the target time  $T$ .

- 
- [1] S. A. Rice and M. Zhao, *Optical Control of Molecular Dynamics* (John Wiley & Sons, New York, 2000).  
 [2] L. Allen and J. H. Eberly, *Optical Resonance and Two-level Atoms* (Dover, New York, 1987).  
 [3] Y. Teranishi and H. Nakamura, Phys. Rev. Lett. **81**, 2032 (1998).  
 [4] J. S. Melinger, S. R. Gandhi, A. Hariharan, D. Goswami, and W. S. Warren, J. Chem. Phys. **101**, 6439 (1994).  
 [5] K. Bergmann, H. Theuer, and B. W. Shore, Rev. Mod. Phys. **70**, 1003 (1998).  
 [6] P. Král, Z. Amitay, and M. Shapiro, Phys. Rev. Lett. **89**,

- 063002 (2002).  
 [7] J. Gong and S. A. Rice, Phys. Rev. A **69**, 063410 (2004).  
 [8] D. J. Tannor and S. A. Rice, J. Chem. Phys. **83**, 5013 (1985).  
 [9] M. Shapiro and P. Brumer, *Principles of the Quantum Control of Molecular Processes* (John Wiley & Sons, New York, 2003).  
 [10] M. C. Gutzwiller, *Chaos in Classical and Quantum Mechanics* (Springer-Verlag, New York, 1990).  
 [11] F. Haake, *Quantum Signatures of Chaos* (Springer-Verlag, Heidelberg, 2001), 2nd ed.

- [12] P. Gaspard, S. A. Rice, H. J. Mikeska, and K. Nakamura, *Phys. Rev. A* **42**, 4015 (1990).
- [13] T. Takami, *J. Phys. Soc. Jpn.* **60**, 2489 (1991).
- [14] T. Takami and H. Hasegawa, *Phys. Rev. Lett.* **68**, 419 (1992).
- [15] J. Zakrzewski and D. Delande, *Phys. Rev. E* **47**, 1650 (1993).
- [16] T. Takami, J. Maki, J. Ooba, T. Kobayashi, R. Nogita, and M. Aoyagi, *J. Phys. Soc. Jpn.* **76**, 013001 (2007), nlin.CD/0611042.
- [17] T. Takami, *Phys. Rev. Lett.* **68**, 3371 (1992).
- [18] T. Takami, *Prog. Theor. Phys. Suppl.* **116**, 303 (1994).
- [19] T. Takami, *Phys. Rev. E* **52**, 2434 (1995).
- [20] M. Wilkinson, *J. Phys. A: Math. Gen.* **21**, 4021 (1988).
- [21] M. Wilkinson and M. A. Morgan, *Phys. Rev. A* **61**, 062104 (2000).
- [22] G. M. Huang, T. J. Tarn, and J. W. Clark, *J. Math. Phys.* **24**, 2608 (1983).
- [23] H. A. Rabitz, M. M. Hsieh, and C. M. Rosenthal, *Science* **303**, 1998 (2004).
- [24] A. P. Peirce, M. A. Dahleh, and H. Rabitz, *Phys. Rev. A* **37**, 4950 (1988).
- [25] M. Abe, Y. Ohtsuki, Y. Fujimura, and W. Domcke, *J. Chem. Phys.* **123**, 144508 (2005).
- [26] S. Suzuki, K. Mishima, and K. Yamashita, *Chem. Phys. Lett.* **410**, 358 (2005).
- [27] W. Zhu, J. Botina, and H. Rabitz, *J. Chem. Phys.* **108**, 1953 (1998).
- [28] Y. Ohtsuki, W. Zhu, and H. Rabitz, *J. Chem. Phys.* **110**, 9825 (1999).
- [29] T. Takami and H. Fujisaki, *J. Phys. Soc. Jpn.* **73**, 3215 (2004), nlin.CD/0402003.
- [30] T. Takami, H. Fujisaki, and T. Miyadera, *Adv. Chem. Phys.* **130 part A**, 435 (2005), nlin.CD/0402005.
- [31] J. J. Sakurai, *Modern Quantum Mechanics* (Addison-Wesley, 1994), 2nd ed.
- [32] W. Zhu and H. Rabitz, *J. Chem. Phys.* **110**, 7142 (1999).
- [33] K. Yamanouchi, *Science* **295**, 1659 (2002).
- [34] T. Yasuike and K. Someda, *J. Phys. B* **37**, 3149 (2004).
- [35] E. Ott, *Chaos in Dynamical Systems* (Cambridge University Press, Cambridge, 2002), 2nd ed.
- [36] C. D. Schwieters and H. Rabitz, *Phys. Rev. A* **44**, 5224 (1991).
- [37] H. Fujisaki, Y. Teranishi, A. Kondorskiy, and H. Nakamura, *Semiclassical approaches to controlling chemical reaction dynamics* (2003), quant-ph/0302025.
- [38] A. Kondorskiy, G. Mil'nikov, and H. Nakamura, *Phys. Rev. A* **72**, 041401(R) (2005).
- [39] J. Gong and P. Brumer, *Phys. Rev. Lett.* **86**, 1741 (2001).
- [40] J. Gong and P. Brumer, *Ann. Rev. Phys. Chem.* **56**, 1 (2005).
- [41] T. Takami and H. Fujisaki, unpublished (2006).